Visualization of laser-induced breakdown and ignition

Ying-Ling Chen and J. W. L. Lewis

Center for Laser Applications, The University of Tennessee Space Institute, 411 B. H. Goethert Parkway, Tullahoma, Tennessee 37388-8897
ychen@utsi.edu, jlewis@utsi.edu

Abstract: Laser-induced gas breakdown and ignition of atmospheric pressure NH_3/O_2 mixtures are investigated. The nanosecond-pulsed, 1064-nm Nd:YAG laser is used to create the cascade-type optical breakdown. The post-breakdown plasma and ignition are studied using spectroscopic techniques that include spontaneous emission and NH planar laser-induced fluorescence (PLIF). These time-resolved two-dimensional images provide not only radiative and gas dynamic information but also the space-time loci of the temperature and transient species concentrations. The results provide an understanding of the plasma kernel dynamics and the flame development that is essential to verify on-going simulation modeling of laser-ignition.

OCIS codes: (140.3440) Laser-induced breakdown; (190.1900) Diagnostic applications of nonlinear optics; (300.6500) Spectroscopy, time-resolved; (280.1740) Combustion diagnostics; (999.9999) Laser-induced ignition

References and links

1. A.H. Lefebvre, *Gas Turbine Combustion* (Hemisphere Publishing Corporation, New York, 1983), pp 221-256.
2. B. Lewis and G. von Elbe, *Combustion, Flames, and Explosions of Gases*, Third Edition, (Academic Press, Orlando, FL) pp 333 - 361.
3. D. R. Ballal and A. H. Lefebvre, "The influence of flow parameters on minimum ignition energy and quenching distance," In *15th International Symposium on Combustion*, (Combustion Institute, Pittsburgh, 1974), pp.1473-1480.
4. P. S. Tromans and R. M. Furzeland, "An analysis of Lewis number and flow effects on the ignition of premixed gases," in *21st International Symposium on Combustion*, (Combustion Institute, Pittsburgh, 1986), pp.1891-1897.
5. G. G. DeSoete, "The influence of isotropic turbulence on the critical ignition energy," in *13th International Symposium on Combustion*, (Combustion Institute, Pittsburgh, 1970), pp. 735-743.
6. F. J. Weinberg and J. R. Wilson, "Preliminary investigation of the use of focused laser beams for minimum ignition energy studies," Proc. Roy. Soc. Lond. Series A **321**, 41-52, (1971).
7. G. F. Carrier, F. E. Fendell, and M. S. Chou, "Laser-initiated conical detonation wave for supersonic combustion. III," AIAA, *28th AIAA/SAE/ASME/ASEE joint propulsion Conference and exhibit*, (Nashville, 1992), paper 92-3247
8. R. G. Kingdon and F. J. Weinberg, "Effect of plasma constitution on laser ignition energies," in *16th international Symposium on combustion*, (Combustion Institute, Pittsburgh, 1976). pp. 747-756
9. J. A. Syage, E. W. Fournier, R. Rianda, and R. B. Chen, "Dynamics of flame propagation using laser-induced spark initiation: ignition energy measurements," J. Appl. Phys., **64**, 1499-1507, (1988).
10. J. H. Lee and R. Knystautas, "Laser spark ignition of chemically reactive gases," AIAA J. **7**, 312-317, (1969).
11. H. M. Thompson, J. W. Daiber, and R. G. Rehm, "Two-dimensional growth of laser-driven waves in a hydrogen free jet," J. Appl. Phys., **47**, 2427-2432, (1976).
12. V. F. Klimkin, R. I. Soloukhin and P. Wolansky, "Initial stages of a spherical detonation directly initiated by a laser spark," Combust. Flame, **28**, 61-66, (1977).
13. B. E. Forch, and A. W. Miziolek, "Ultraviolet laser ignition of premixed gases by efficient and resonant multiphoton photochemical formation of microplasma," Combust. Sci. Tech. **52**, 151-159, (1987).
14. B. E. Forch, and A. W. Miziolek, "Laser-based ignition of H_2/O_2 and D_2/O_2 premixed gases through resonant multiphoton excitation of H and D atoms near 243 nm," Combust. Flame, **85**, 254-262, (1991).

#34969 - $15.00 US Received August 10, 2001; Revised September 23, 2001

15. M.-S. Chou, F. E. Fendell, and H. W. Behrens, "Theoretical and experimental studies of laser-initiated detonation waves for supersonic combustion," Proc. SPIE, **1862**, 45-58 (1993).
16. R. A. Hill, "Ignition-delay times in laser-initiated combustion," Appl. Opt., **20**, 2239-2242, (1981).
17. D. H. Plemmons, "Laser-spark ignition and the NH radical," (PhD thesis, The University of Tennessee Space Institute, 1996)
18. J. D. Few and J. W. L. Lewis, "Gas turbine engine photon ignition system," (U.S. Patent number 4,947,640, Aug. 14, 1990)
19. J. D. Few and J. W. L. Lewis, "Laser-initiated non-linear fuel droplet ignition," U.S. Patent number 5,485,720, Jan. 23, 1993, Patent number 5,404,712, April 11, 1995, Patent number 5,497,612, March 12, 1996, Patent number 5,524,429, June 11, 1996.
20. Y.-L. Chen, J.W.L. Lewis, and C. G. Parigger, "Spatial and Temporal Profiles of Pulsed Laser-Induced Air Plasma Emissions," J. Quant. Spectr. & Radiat. Trans., **67**, 91-103, (2000).
21. Y.-L. Chen, J. W. L. Lewis, and C.G. Parigger, "Probability Distribution of Laser-Induced Breakdown and Ignition of Ammonia," J. Quant. Spectr. & Radiat. Trans., **66**, 41-53, (2000).
22. I.G.Dors, C.G.Parigger, and J.W.L.Lewis, "Fluid Dynamics Effects Following Laser-Induced Optical Breakdown," *38th Aerospace Sciences Meeting and Exhibit*, paper AIAA 2000-0717, (Reno, NV 2000).
23. R. J. Kee, J. F. Grcar, M. D. Smooke, and J. A. Miller, A FORTRAN program for modeling steady one dimensional flames (Technical Report SAND85-8240, Sandia National Laboratories, 1985)
24. R. G. Root, "Modeling of the post breakdown phenomena," in L. J. Radziemski and D. A. Cremers, editors, "Laser-induced plasma and applications," (Marcel Dekker, Inc. New York, 1989)
25. D.H. Plemmons, C. Parigger, J.W.L. Lewis and J.O. Hornkohl "Analysis of Combined Spectra of NH and N2," Applied Optics, Vol. **37**, No. 12, pp. 2493-2498, (April 1998).
26. E. Sher, J. Ben-Ya'ish, and T. Kravchik, "On the birth of spark channels," Combust. Flame, **89**: 186-194, (1992).
27. T. Kravchik and E. Sher, "Numerical modeling of spark ignition and flame initiation in a quiescent methane-air mixture," Combust. Flame, **99**: 635-643, (1994).
28. J. O. Hornkohl, C. Parigger, and J. W. L. Lewis, "On the use of line strengths in applied diatomic spectroscopy," in Optical Society of America for presentation in *the conference on Laser Applications to Chemical and Environmental Analysis*, (March 1996).
29. J. O. Hornkohl, C. Parigger, and J. W. L. Lewis, "Computation of Synthetic diatomic spectra," in *Laser Applications to Chemical Analysis*, OSA 1994 Technical Digest Series, **5**: 234-237, (Washington, DC, 1994).

1. Introduction

Throughout the past half-century the use of electric spark ignition has been dominant for gas turbine combustion engines [1], and an extensive body of knowledge was developed to obtain an understanding of the ignition phenomena. As examples, the minimum ignition energy and optimal spark power were determined for a range of fuel/oxidizer mixtures, gas flow conditions, and fuel droplet sizes and size distribution functions for two-phase mixtures. Additionally, the effects of the flow field on the ignition process were studied for both laminar and turbulent flows [1-5]. However, it is easily seen that the necessary location of the spark plug on the combustor wall results in non-stoichiometric mixtures at the plug site and the production not only flame on the combustor walls at onset of ignition but also wall-mediated soot formation. Laser ignition offers an attractive alternative in that stoichiometric combustion can be achieved in desired spatial regions distant from the walls by focusing the radiative energy and power density required for breakdown and ignition. However, the published research work of the laser ignition of gas/vapor mixtures is limited. The previous studies of gas/vapor ignition include the macroscopic measurements of the minimum ignition energy [6-15] and the ignition delay time [16, 17] for various laser sources and ignition mechanisms. Further, the laser-ignition research of the two-phase mixtures has been mostly proprietary and necessarily described by both U.S. and foreign patents of Lewis and Few [18, 19]. In our previous work, we investigated the effects in gas/vapor mixtures of the flow environment on the formation and development of the laser spark [20, 21]. Although hydrocarbon fuels are clearly of interest, the work of Refs. [20, 21] used mixtures of ammonia and oxygen to take advantage of this mixture's simplicity of chemical kinetics and spectroscopic features relative to that of hydrocarbon and oxygen. The laser focusing effects

#34969 - $15.00 US Received August 10, 2001; Revised September 23, 2001

and subsequent spatial development of the initial plasma within the first 25 nsec were presented. The temperature profile of the initial plasma depends on the laser-focusing geometry and the temporal profile of energy deposition process. The initial plasma was observed to develop, depending on the laser irradiance, with a speed greater than ten km/sec toward the laser source. The probability distribution function of laser breakdown and ignition were also examined for the gas flow environment and laser conditions. These results were used to provide the initial condition required for the computational modeling of laser ignition [22].

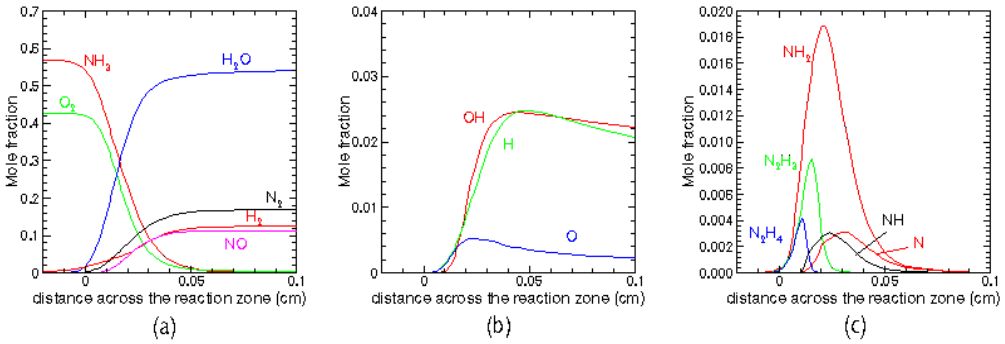

Fig. 1 mole fractions of species across the flame front of ammonia/oxygen combustion. Calculation were performed using Sandia Chemkin code [23]

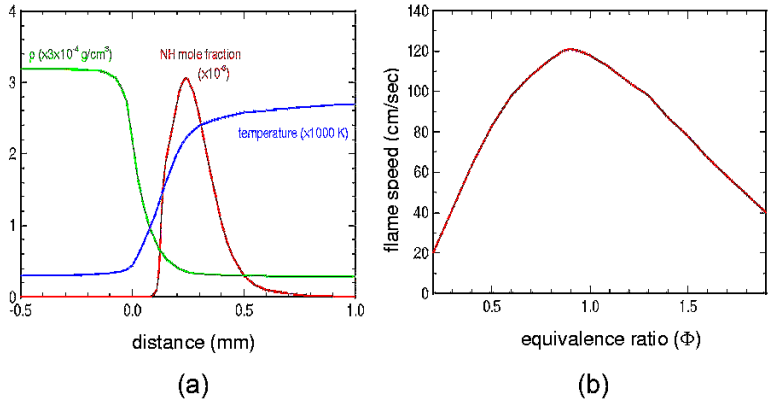

Fig. 2 calculation results of the 1-dimensional free propagate ammonia/oxygen flame (a): flame temperature ($\times$ 1000 K), mass density ($\times 3 \times 10^{-4}$g/cm^3), and NH mole fraction ($\times 10^{-3}$) across the stoichiometric NH_3/O_2 flame-front. (b): flame speed vs. fuel/oxidant equivalence ratio of premixed ammonia/oxygen flame

The variation in time of the temperature and the location and structure of the flame front of the developing ignition process provide useful measures of comparison with computational predictions that are in progress. These measures were obtained using excitation scans of laser-induced fluorescence (LIF), planar laser-induced fluorescence (PLIF), and spontaneous emission. In both LIF and PLIF, a probe laser produced resonant excitation of a selected molecular species and the fluorescence was collected by a spectrometer and a CCD camera, respectively. The combustion intermediate NH was chosen as the species of interest. From calculations using ChemKin code [23], the significance of NH in the ammonia/oxygen combustion is shown. Fig. 1 shows calculated flame properties in a one-dimensional freely

#34969 - $15.00 US
Received August 10, 2001; Revised September 23, 2001

propagating NH_3/O_2 flame. On the left hand side of the chemical reaction zone, the unburned gases (ammonia and oxygen) are premixed in a fuel/oxidant mole ratio of 4/3, which corresponds to the stoichiometric state, or equivalence ratio of one. Together with other N_xH_y species, the NH density is produced and consumed in the flame front. Figure 2(a) shows the temperature and mass density across the flame front. NH exists in the region corresponding to temperature range of ~1400 to 2600 K. Fig. 2(b) shows the flame speed vs. the equivalence ratio. The N_xH_y radicals produced from the chemical reaction appears only for a short time, between tens to hundreds μs, after reaction initiation. Consequently, the they exist only inside the thin layer of the flame-front thickness of 0.1 to 0.4 mm. Monitoring the spatial and temporal formation of a transient species provides significant information of the gas-dynamics as well as the chemistry in the ignition process. This feature of NH and its well known spectral properties indicate its use for this study.

A qualitative summary of these laser breakdown and induced ignition results is useful. For ammonia breakdown using a 1064-nm laser pulse of 6.5 nsec and approximately 30 mJ, the initial plasma formation occurs in the first 20 nsec following breakdown as a laser-supported radiation wave [20, 22, 24]. The optically thick plasma absorbs practically all the incident laser energy, and the growth of the plasma wave propagates with a speed of ~20 – 80 km/sec. By the end of this period, the initial plasma is formed along the optical axis with a length of ~ 1 mm and a diameter of 70 μm near the focal point and 200 μm on the laser side. Inside the kernel, the temperature and pressure are on the order of 100,000 K and 1000 bar, respectively. The mass density remains near 1 amagat. At about 1 μsec after the pulse, the initial plasma is oval-shaped with a length of ~ 2mm and a diameter of ~ 1.5 mm near the laser side. For this estimate, the kernel size is estimated from the shell of NH molecular radiation that is produced by the planar laser-induced fluorescence (PLIF) of the NH A – X transition. The pressure has dropped to approximately 2 bar. At ~ 2-3 μsec, the induced shock wave separates from the kernel and propagates outward. The roughly cylindrically shaped kernel is about 3 mm long with a diameter of 2 mm, which implies a volume expansion of the kernel of about 1000 from its initial size. The rarefaction wave from the shock decreases the pressure within the kernel to less than 1 bar. As shown by Rayleigh scattering and NH PLIF images, the breakdown kernel is optically thin in the PLIF excitation and emission regions. Further, inside the hot kernel, NH ground electronic state molecules appear to be formed in a hollow shell near the kernel boundary and to be characterized by temperatures in the region of ~ 2500 – 2800 K. From 10 - 50 μsec, no further increase in kernel size occurs, and the pressure slowly recovers to 1 bar. However, a toroidal flow feature begins to form in this time frame. An asymmetric pressure force and gas motion appear inward along the axis and outward in the radial direction. This motion starts earlier and stronger in the backside of the kernel and is observed later and weaker in the front side. When the motion from both sides of the kernel meet and when the stronger one from the backside overcomes the weaker frontside force and pushes the core of the kernel toward the front, the backstreaming effect appears. The gas dynamics that leads to the backstreaming effect is examined and modeled elsewhere [22]. When the optical breakdown takes place in a combustible gas mixture, the enthalpy release of the chemical reactions contributes significantly to the developing hot kernel as early in time as 20 μsec. A successful ignition requires the establishment of a proper temperature gradient to support the exothermic reactions and to initiate a self-sustained flame front. The minimum ignition energy in laser-induced breakdown depends on the focusing optical geometry and the energy losses before the initial plasma develops into a proper ignition kernel. As observed in our laser-ignition experiments, formation of a closed NH-molecule shell seems to be one of the necessary conditions for a successful ignition [21]. The NH shell may ensure a proper temperature gradient and/or a suitable fuel/oxidant combination for the subsequent chemical reactions.

The results of Ref. [20] have shown the sensitivity of the computational results to various assumptions, including the initial conditions such as the laser energy deposition and its spatial

#34969 - $15.00 US Received August 10, 2001; Revised September 23, 2001

profile, as well as specific reaction model parameters. Also, Ref. [21] has shown the importance of the formation of the NH ground electronic state species. Therefore, validation of the computational model requires detailed, quantitative space-time maps of the temperature and NH radical concentration, and this work addresses this need.

2. Experiment

The experimental arrangement is shown in Fig. 3. A 6.5-nsec pulsed Nd:YAG laser was used to create optical breakdown in laminar ammonia/oxygen flow. The Nd:YAG laser is Q-switched and emits 1.064 μm with output energy of typically 100 mJ and repetition rate of 10 Hz. While maintaining a fixed polarization state, the incident laser energy was controlled by a pair of polarizers. The laser beam was then expanded by two lenses to a beam-width about two cm, and breakdown was generated by focusing the expanded laser pulse using an antireflection-coated 10 cm-focal-length lens. Two energy meters were used to record each laser pulse's incident beam energy, the energy transmitted through the plasma, and the shot-to-shot energy fluctuation of laser output. The systematic errors of both energy meters and fluctuation of laser output were obtained to be less than 0.3 and 1 percent.

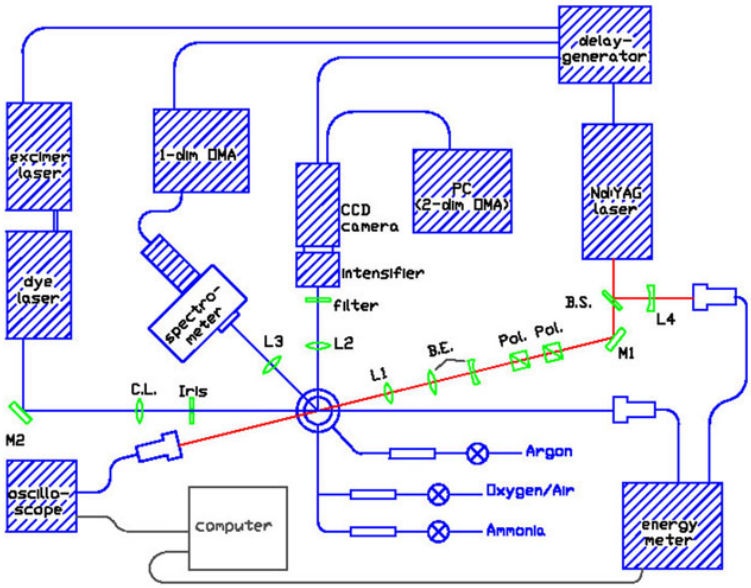

Fig. 3 Experiment geometry of PLIF, B.S. = beam splitter, E1 and E2 = energy meter, M = mirror, Pol. = polarizer, B.E. = beam expander, L = lens, C.L. = cylindrical lens

The 10 Hz repetition rate Nd:YAG laser was focused to achieve breakdown 1 cm above the McKenna burner source of the premixed gases. The flow speed of the gases was 6.0 cm/sec to obtain laminar flow, and an annular sheath of argon flow surrounded the core flow. The argon flow speed was matched to that of the core flow to stabilize the core flow and to minimize its mixing with the ambient atmosphere.

The equipment for the spectroscopic diagnostics includes a probe tunable dye laser, spectrometer, and an intensified-CCD camera system. For the acquisition of the spontaneous radiation images, an intensified-CCD camera and the two-dimensional optical multi-channel analyzer (EG&G PARC OMA4, Model No. 1530-CUV) were used to record the images of the kernel in the direction of 76˚ with respect to the Nd:YAG laser beam. A narrow band-pass filter ($\Delta\lambda \sim 10$ nm) centered at 337 nm was used to isolate spectrally the NH(A-X) $\Delta v = 0$

#34969 - $15.00 US Received August 10, 2001; Revised September 23, 2001

radiation. To prevent multi-species excitation and/or interference in signal collection, spectrum of several potential species were calculated and examined [23]. The transmission functions of the filters used and the synthetic spectra of NH, OH, and N_2 are shown in Fig. 4. The detected spontaneous radiation images from the plasma kernel included a certain percentage of the N_2 Second Positive radiation through the narrow band-pass filter. The combined spectra of NH and N_2 has been investigated in a previous study [25]. For the experiments of the NH PLIF, an excimer-pumped dye-laser system was tuned to resonantly excite NH molecules in the pose-breakdown kernels at selected delay time. The dye laser beam was focused into a sheet beam and transmitted through the center of the plasma kernel with an angle of 14˚ with respect to the optical axis of the Nd:YAG laser beam, and the induced fluorescence signals were imaged into the CCD camera system. When the PLIF images were acquired for the purpose of the two-dimensional temperature calculation, a broad band-pass filter was used (see Fig. 4) to replace the narrow band filter. The two-dimensional OMA was calibrated to ensure linearity of the response. The Rayleigh (or Mie) scattering images were obtained by tuning the dye-laser to the off-resonant wavelengths of the molecules.

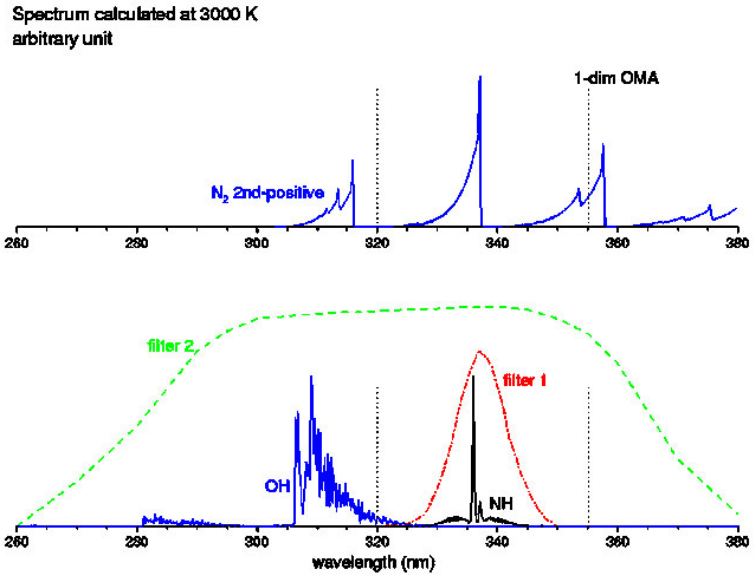

Fig. 4 Synthetic spectra of NH(A-X), OH(A-X) and N_2 (2^{nd} positive), and relative transmissions of narrow band-pass filter for NH(A-X) PLIF experiment, broad band-pass filter for NH temperature experiment, and 1-D OMA for excitation-scan experiment

In the experiments of the laser-induced fluorescence excitation scan, the 10 Hz narrow band ($\Delta\lambda < 0.002$ nm or $\Delta\nu < 0.2$ cm^{-1}) tunable dye-laser was scanned across the P-branch of the NH(A-X) transitions from 337 to 344 nm with the step-speed of 0.001 nm/sec. The focused dye-laser sheet beam passed through each breakdown kernel at a 5-μsec delay time after the Nd:YAG laser induced the breakdown. The signal of the induced NH fluorescence was focused on the entrance slit of a spectrometer (Jarrell-Ash Monospec27, with photodiode array: EG&G PARC, Model No. 1423), and the one-dimensional OMA (1D-OMA: EG&G PARC, Model No. 1460) recorded it simultaneously with the laser scanning. The spectral detection range of the spectrometer in the experiment was selected to be 320-355 nm, as the dotted lines shown in Fig. 4.

#34969 - $15.00 US Received August 10, 2001; Revised September 23, 2001

3. Results and discussion

3-1. NH spontaneous emission and planar laser-induced fluorescence

Time-resolved images of NH spontaneous radiation and NH PLIF in laser-induced ammonia breakdowns are shown in Fig. 5 and Fig. 6 (a). In these two figures, each image has the scale of 4 mm by 4 mm. The Nd:YAG laser pulse was incident from the left for each image with an incident and absorbed pulse energy of 32 and 26 mJ, respectively. The burner is located at the

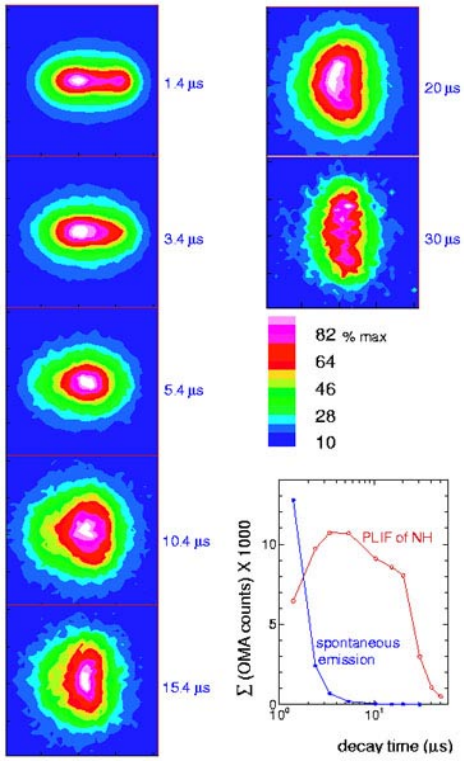

Fig. 5 Images of NH (A-X) spontaneous emission in laser-induced ammonia breakdown. Nd:YAG laser was incident from the left of each image. Each time-resolved image size: 4 mm × 4 mm

lower side, 10 mm below the breakdown axis. The radiation at the earliest 2 μsec contains a large amount of continuum spectrum that results mostly from the recombination process of the ions and electrons. After a couple of microseconds, the spontaneous emission images illustrate the spatial distribution of the NH molecules in the $A^3\Pi_i$ electronic excited state. The PLIF images, on the other hand, present the location of the ground state ($X^3\Sigma^-$) NH populations. Instead of residing in the center of breakdown kernel as do the excited state species, the ground state NH molecules are located in a layer surrounding the hot gas kernel. The fluorescence intensity of NH(X) in the center of the kernel is less than one half of that in the outer shell layer. The different NH distribution in these two figures can be explained. First, the PLIF images are spatially resolved whereas the spontaneous emission is integrated over the optical depth. Second, the spontaneous emission of NH from the excited electronic state depends more heavily on the temperature than the ground-state NH in PLIF. Assuming

#34969 - $15.00 US Received August 10, 2001; Revised September 23, 2001

that the concentration of the ground state NH(X) in the center of the kernel is one half of that near the boundary (or flame front), and that the molecular temperature is approximately 3300K and 2700K at these two locations, respectively, for the condition of local thermal equilibrium, the population of the electronic excited state NH(A) in the core would be at least an order larger than in the boundary. Therefore, the information carried in the spontaneous emission images is more likely to be determined by the temperature gradient than the NH distribution. The plot in the lower-right corner of Fig. 5 shows the comparison of the magnitudes of the spontaneous emission from the excited state NH(A) and the fluorescence signal from the ground state NH(X). When the kernel temperature drops after 2 μsec, the density of the ground state NH molecules increases and maintains its magnitude for about 40 μsec of time before decaying. When ammonia is mixed with oxygen, the intermediate NH can be produced through the chemical reactions. When ignition happens, the NH fluorescence signal level increases after ~10 μsec and maintains the magnitude throughout the ignition process.

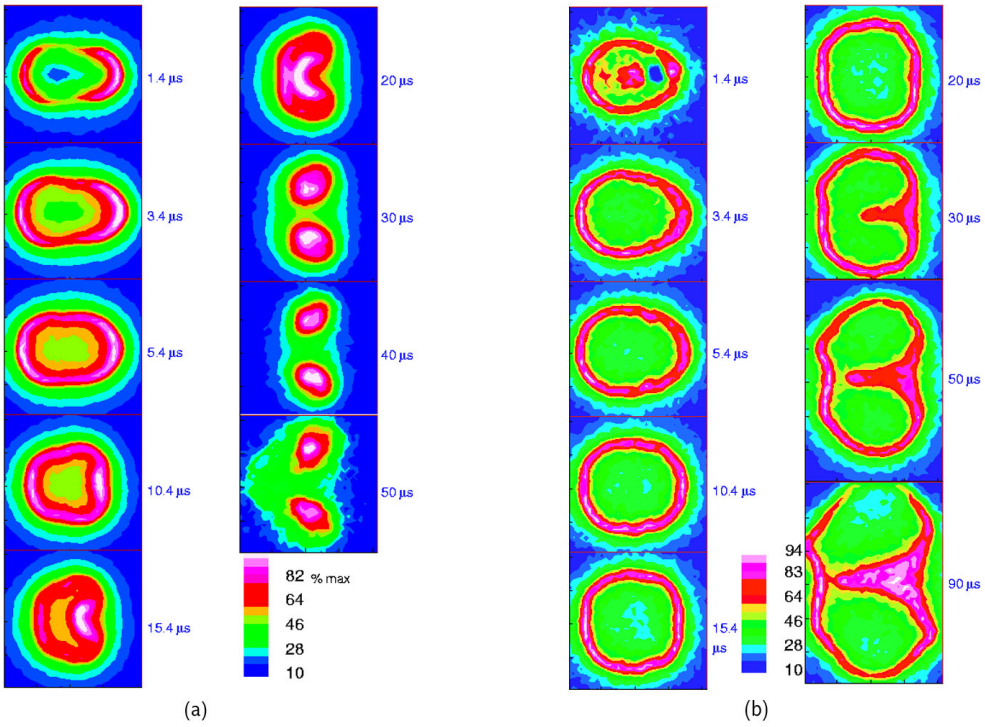

Fig. 6 Images of NH (A-X) planar laser-induced fluorescence in (a) laser-induced ammonia breakdown, (b) laser-induced ammonia/oxygen ignition, images scale: 4 mm × 4 mm for all except the last 2 images, 4 mm × 6 mm.

The toroidal shape of plasma kernel appears to be a universal phenomenon of both short-pulse electric and laser sparks. When the initial plasma expands, opposite to the expansion direction, the gas along the axis moves inward toward the center of hot kernel. The development of the electric kernel is symmetric along its axis while the laser spark is always asymmetric due to the optical focusing geometry. The force from the front (the focal point side) is always stronger than the backside and the cold ambient air will push through the kernel toward the laser incoming direction eventually if no strong chemical reactions involve.

#34969 - $15.00 US
Received August 10, 2001; Revised September 23, 2001

This phenomenon is due to the asymmetry of the developed pressure gradient and is described by the simulation results [22]. In the experiment, this back-streaming structure of the kernel appears around 10 μsec of delay time in both sets of images, although the feature is not very clearly shown from the spontaneous radiation images. From the PLIF images, we can observe the initiation of the toroidal geometry from both sides of the kernel. The stronger pressure force pushing the plasma kernel from the back (right) appears at 10 μsec of time, and a weaker motion from the front (left) side appears at approximately 20 μsec of delay time. In the radial direction, too, the kernel seems to expand more significantly in the back than in the front. A tunnel is formed along the axis around 40-μsec delay time in the PLIF images.

The PLIF images of laser ignition are shown in Fig. 6 (b). The experimental conditions are the same as that in Fig. 6 (a) except that the stoichiometric ammonia/oxygen ($\Phi = 1.0$) flow is combustible and chemically reacts following ignition by the laser pulse. The sizes of images corresponding to the 50- and 90-μsec delay are 4 mm times 6 mm. The rest of images are 4 mm by 4 mm as before. As in Fig. 6 (a), the image recorded at 1.4 μsec of delay time suffers from strong background noise from the spontaneous emissions in the center of the kernel, and cannot illustrate the proper intensity around this location. The shapes of the expanded plasma kernels of the ignition and non-ignition breakdowns clearly have developed differently in the earliest 2 μsec. In contrast to the pure ammonia breakdown, the size of the hot kernel of the combusting mixture is larger, and the NH-molecule layer is thinner in the ignition kernel, which imply a stronger expanding pressure and temperature gradient than found for the pure ammonia case. The fluorescence signal in the core of the ignition kernel is apparently weaker than for the pure ammonia breakdown due to the lower mole fraction of the participating N and H atoms. Around 10 to 20 μsec of time, the kernel front has developed into a self-sustained flame front. As a result, the NH molecules are supplied through the chemical reactions in ammonia/oxygen flame, and the total intensity of NH fluorescence continuously increases instead of decaying away as in the pure ammonia breakdown.

As in Fig. 6 (a) and Fig. 6 (b), a significant concentration of the ground state NH molecules seems to exist in the interface between the hot-gas kernel and the ambient ammonia gas, which suggests a possible formation procedure through the combustion reaction chemistry rather than the recombination of atoms in the kernel. The feature of the NH shell layer appears as early as one microsecond of time from the laser pulse. The generation of NH through heating requires the breaking of two N-H bonds in the ambient ammonia molecules. Through the recombination process, on the other hand, NH molecules could appear in a very early time following the breakdown. In Fig. 6 (b), the ignition delay time at the $\Phi = 1$ condition is observed around 20 μsec (determined by the tuning point of NH free-radical density), which indicates, roughly, the beginning stages of combustion or chemical reactions. In the very early period of time (< 5 μsec), the atom recombination process is probably the major supplier of the NH(X) molecules. The temperature dependence of recombination-generated molecules may explain the cause of the NH distribution near the surface of the hot gas kernel. In the other words, the density of ions, electrons, atoms, and molecules inside the breakdown kernel are dependent on the local temperature. The NH molecule is more difficult to form near the very hot core than in the outer area where the temperature favors its formation. Numerical analyses of the development of electric sparks show the strong dependence of the temperature and the concentration of various transient species, and the molecular shell layers are also predicted [26, 27].

A notable difference of NH density between breakdown and ignition in Fig. 6 appears in the back streaming locations. For the ignition case, NH is produced by the chemical reaction in the flame front, which is determined by the fuel/oxidizer ratio and temperature. This strong temperature dependence of NH density will be shown experimentally in Fig. 8 of ammonia breakdown in the followed section.

#34969 - $15.00 US Received August 10, 2001; Revised September 23, 2001

3-2. Temperature and concentration maps

The NH rotational temperature is determined using the spectroscopic technique of LIF excitation scan. In the pure ammonia breakdowns, the measured and computed excitation spectra of NH molecules at 5-μsec delay time are shown in Fig. 7. The NH molecules contribute fluorescence signal across the area of excitation of the probe laser beam, and across this area there exists a corresponding temperature distribution. To reduce the strong background noise in the wavelength range of the probe laser, only the fluorescence signal in

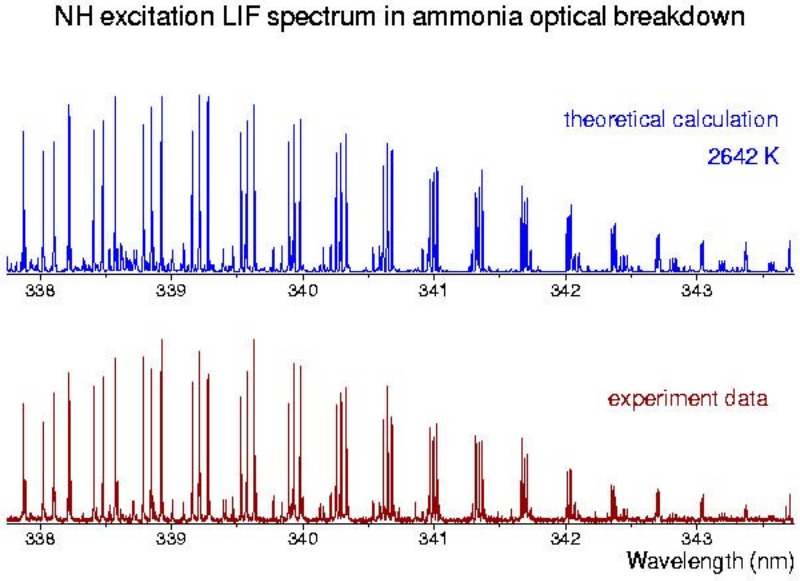

Fig. 7 NH excitation spectra in atmospheric-pressure laser-induced ammonia breakdown

Q- and R-branches of the (0-0) band of NH was collected in this measurement. Therefore, the excitation spectrum is used to determine, or locate, some clean, non-overlapped transition lines for the temperature measurements and to determine if multi-species excitation has occurred, rather than determining the temperature itself. To prevent multi-species excitation, the computed spectral lines of electronic transitions of molecules N_2 and OH were carefully compared with measured and computed NH spectra (see Fig. 4). No significant involvement of multi-species excitation was found in either experiments of the atmospheric pressure NH_3/O_2 flames or the pure NH_3 breakdowns. Ten selected transition lines in the P-branch of NH(A-X) $\Delta v = 0$ were used in the two-dimensional temperature measurements of ammonia breakdowns. Corresponding to each of the selected excitation lines, an off-resonant point was chosen for the background determination (see the excitation spectrum in Fig. 7). The parameters of these transition lines that were used are listed in Table 1 [28, 29].

The subscripts of the transition types P_{ij} in Table 1 indicate the triplet splitting of the corresponding rotational states in the upper ($A^3\Pi_i$) and lower ($X^3\Sigma^-$) electronic states. The given term values are the lower-state energy levels of the corresponding transitions. The variation of Einstein A coefficient between the selected transitions is very small. Over the wavelength range of ten excitation lines, the pulse energy of the probe dye laser is not constant. The output power varies over this spectral region by about 10 %. For excitations in the linear optical interaction regimes, since the fluorescence intensity is proportional to the laser intensity, the wavelength-variation of the dye laser power can be easily corrected between these ten transitions. To ensure that the LIF thermometry is applied in the linear

#34969 - $15.00 US Received August 10, 2001; Revised September 23, 2001

regime, saturation irradiance in the ammonia breakdown needs to be determined prior to the temperature measurements. Measurements of the saturation intensity were carried out in both the ammonia/oxygen flame and the pure ammonia breakdown. For the acquisition of the two-dimensional temperature images, the irradiance of the dye-laser sheet beam was operated at about one half of the measured saturation irradiance. Each of the ten PLIF images used to determine the temperature maps was acquired by accumulating fluorescence signals over 500 breakdowns events to achieve the spatially stable distribution. The background images, as mentioned, were subtracted by tuning the dye-laser wavelength to off-resonance for each

Table 1. Parameters used in the laser-induced fluorescence thermometry

Type	λ (nm)	N" / J"	term" (cm^{-1})	A (sec^{-1})	Bkg. λ (nm)
P_{33}	339.5275	10 / 09	3399.77	1.1367E+06	339.488
P_{11}	339.6293	10 / 11	3398.74	1.1013E+06	339.488
P_{11}	339.9804	11 / 12	3749.29	1.1103E+06	340.020
P_{33}	340.2539	12 / 11	4131.13	1.1422E+06	340.404
P_{33}	340.6117	13 / 12	4541.41	1.1433E+06	340.502
P_{11}	341.0226	14 / 15	4979.33	1.1244E+06	341.143
P_{33}	341.3171	15 / 14	5448.67	1.1434E+06	341.237
P_{22}	341.6862	16 / 16	5944.69	1.1244E+06	341.546
P_{33}	342.0100	17 / 16	6467.81	1.1417E+06	341.960
P_{22}	342.0281	17 / 17	6467.90	1.1254E+06	341.960

transition line. The scale of each PLIF image in the temperature measurements is 4.42 mm in both horizontal and vertical directions, and the images were recorded in 70 times 70 pixels. By applying the Boltzmann plot at each recorded point (pixel), the two-dimensional temperature images were obtained. Fig. 8 (a) shows the time-resolved temperature images with incident Nd:YAG laser energy of 32 mJ, where a stable breakdown and absorption is expected. The average deviations of linear fitting over the whole temperature image are about 2 -- 4 per cent. The region with largest fluorescence signal around the NH molecular shell layer has the smallest percentage of fitting error. In the center of the kernel, the uncertainty is greater due to the larger background noise from the spontaneous emission. Also, outside the kernel, the NH fluorescence reduces dramatically, thereby resulting in an increase of the uncertainty of the Boltzmann plot. A typical Boltzmann plot of a single recorded point is shown in Fig. 9. The error bars in the Boltzmann plot were determined by the analysis of the deviations between single breakdown events, and the magnitude of the measured error bars were used as weighting factors in the least-squares fitting algorithm.

Once the molecular temperature is known, the relative molecular density can be determined. Fig. 8 (b) shows the NH concentration images of the ammonia breakdowns. The absolute concentration values in Fig. 8 (b) was evaluated by comparing fluorescence signals between ammonia breakdown and ammonia/oxygen ignition, and the normalization to the densities obtained in the ChemKin [24] combustion calculation.

Compared with the time-resolved temperature maps shown in Fig. 8 (a), one can clearly see that the NH spontaneous emission images shown in Fig. 5 reveal the thermodynamics of the breakdown kernel instead of the NH population, as we suggested. The ground state NH molecules are mostly populated at spatial locations where the temperature is in the

#34969 - $15.00 US Received August 10, 2001; Revised September 23, 2001

approximate interval of ~2500-2800 K. The calculated temperature outside the NH shell can not be used since the NH density is extremely low in these areas, and the very small detected fluorescence signal could be from the scattering in the imaging process. In our followed experimental studies, OH molecule, which is populated over the entire ignition kernel region, is used to achieve temperature measurement in ignition.

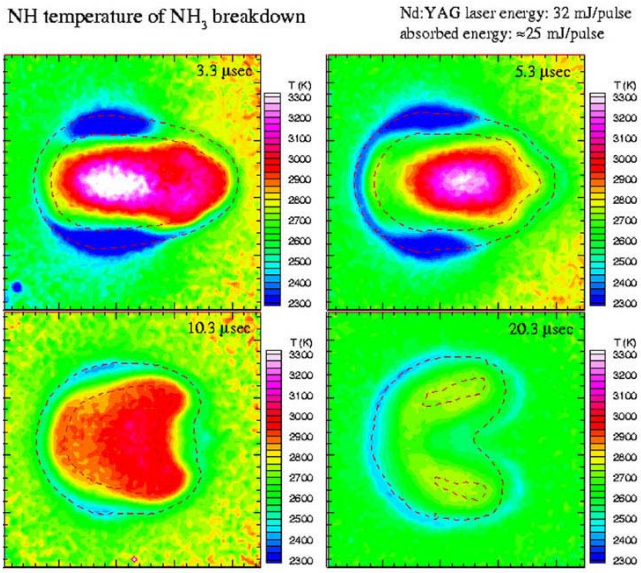

(a)

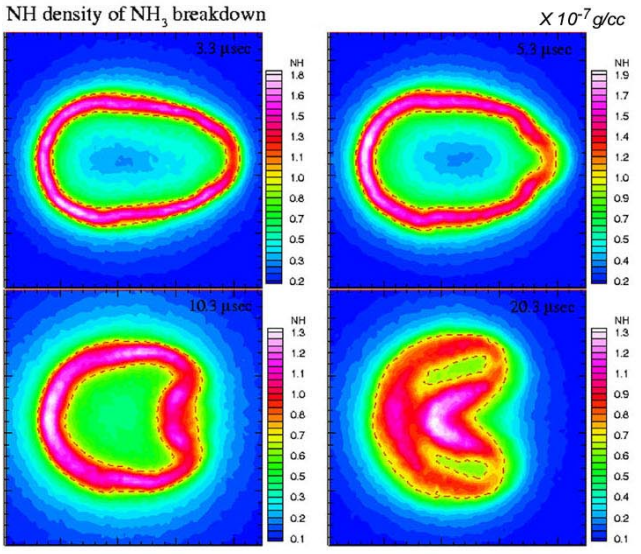

(b)

Fig. 8 . Images of laser-induced breakdown recorded at 3, 5, 10 and 20 µsec after breakdowns were initialed. Nd:YAG laser pulse energy = 32 mJ, (a) time-resolved temperature images, (b) NH concentration images, dotted contour lines show the location where NH concentration equals to 50 % of the peak value. Image side: 4.42 mm by 4.42 mm.

#34969 - $15.00 US
Received August 10, 2001; Revised September 23, 2001

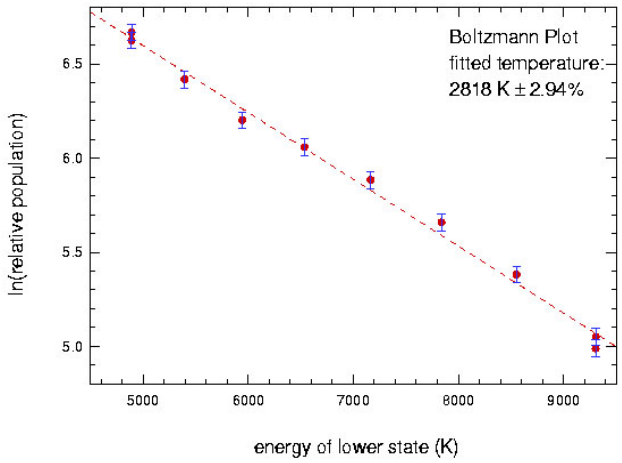

Fig. 9 The Boltzmann plot of a single pixel in 2-dimmensional temperature measurement

4. Summary

Spontaneous emission and PLIF imaging techniques were used to visualize and quantify selected features of the thermochemical and gas dynamic processes of the laser-ignition phenomena. Specifically, observations were obtained immediately following breakdown through onset of combustion for the gas mixture. The time history of the parameters was determined by observing sequential breakdown events and variation of the delay time of image acquisition following laser breakdown. In spite of the stochastic nature of the breakdown process, excellent repeatability was achieved for the results by operating well above the breakdown threshold of the mixture. Temperature results were obtained from PLIF excitation of NH, and for the NH-rich regions, the evolution of the ignition process was observed. Further, the NH concentration results yielded space-time loci of the flame front and its thickness. Both of these results are important for the development and verification of accurate models of laser-ignition of both single- and two-phase mixtures.

#34969 - $15.00 US Received August 10, 2001; Revised September 23, 2001